VALIDATION OF HYPERSPECTRAL IMAGING DATA FROM THE BARRAX TEST SITE WITH BRDF GROUND MEASUREMENTS IN THE REFLECTIVE WAVELENGTH RANGE

Ulrich Beisl[1,2], G. Strub[2], C. Dickerhof[2]

[1]DLR Oberpfaffenhofen
82230 Wessling, Germany
phone: +49-8153-28-1161 Email: Ulrich.Beisl@dlr.de

[2]Remote Sensing Laboratories, Dept of Geography, University of Zurich
Winterthurerstr. 190
8057 Zurich, Switzerland
phone: +41-1-635-5251 Email: gstrub@geo.unizh.ch, corinna@geo.unizh.ch

KEY WORDS: BRDF, hyperspectral, bidirectional, inversion

ABSTRACT

During the DAISEX'99 campaign hyperspectral and multiangular images are taken with the airborne wide angle imaging spectrometer HyMap at the Barrax test site in Spain. For validation purposes, bidirectional ground measurements of dry bare soil, Alfalfa and barley are acquired with the Field Goniometer of the RSL, Zurich.

The image data are atmospherically corrected using the ATCOR4 program developed at DLR. It removes the effects of angular dependent path radiance and atmospheric transmittance in airborne hyperspectral imagery. Using classification and a statistical approach, directional spectra are derived from single images. Thus the image spectra from different viewing angles can be compared with the corresponding goniometric ground spectra by calculating the anisotropy factor.

The potential of correcting bidirectional effects in the whole image is discussed for three different target types.

1 INTRODUCTION

Most current multi- and hyperspectral airborne imaging sensors (e.g., DAIS7915, HyMap, MIVIS) are designed to acquire wide-FOV images, unless a very high spatial resolution is required. Since a spatial resolution of 5 meters is sufficient for many land surface application studies and the flight operation height of non pressurized airplanes without additional oxygen is limited to 4000 meters, one takes resort to wide-FOV systems in order to have a large ground coverage.

The reflectance of many ground surfaces shows anisotropic behaviour already in the angular range of wide-FOV imaging sensors (±30 degrees), which is most prominent if the flight direction is perpendicular to the sun-target-observer plane. Subsequently a large across track illumination gradient is observed, reducing the intercomparability of different portions of the image. Thus routines have been developed to correct this gradient with an overall correction function which does not account for soil-type dependent reflection anisotropy within the image.

To avoid an illumination gradient in the across track direction the flight line is usually directed towards the sun. Together with the need to optimize for a high signal to noise ratio (SNR) while flying at a high solar irradiance (typically at noon), the flight lines are more or less restricted to the north-south direction.

Another source of view angle effects originates from changing view angles due to uneven terrain. This issue is discussed briefly in the conclusions of this paper.

The radiometric calibration is often performed, or at least cross-checked, with ground measurements. To be able to compare the wide-FOV image spectra with ground measurements, the measurements have to be performed at the actual airborne sensor view angle. In this paper we will compare goniometric ground spectra of selected targets with atmospherically corrected image spectra and analyse the angular variation of the reflectance within the image.

In the past twenty years the understanding of the directional reflectance, described by the bidirectional reflectance distribution function (BRDF) (Nicodemus, 1977), has grown enormously. To study the informational content of the BRDF, ESA funded a series of evaluation campaigns (e.g., DAISEX'99 (Berger, 2000)).

2 METHOD

2.1 Data acquisition

Two airborne imaging spectrometers (DAIS7915 and HyMap) are flown on board of a DLR aircraft at the Barrax test site in Spain. The data sets are taken in a cross-shape flight pattern at different times of the day to obtain multiangular information. In this paper only HyMap images are analysed. A ground team performed atmospheric, spectral, thermal and solar flux measurements as well as measurements of soil and vegetation parameters (ESA, 1999).

2.1.1 Goniometric measurement setup

The directional spectral measurements were taken with a GER3700 spectroradiometer (0.4 – 2.5 µm) mounted on the FIeld GOniometer System (FIGOS) of the RSL, Zurich (Sandmeier & Itten, 1999). Since the FOV of the GER spectrometer is limited to 2.7° (approx. 12 cm at a distance of 2 m), only homogeneous surfaces such as dry bare soil (the sample is called S10), alfalfa (V17) and barley (V25) have been selected. The BRDF depends on the viewing geometry and on the illumination geometry. Therefore measurements have to be performed throughout the day to fully describe the BRDF. Up to nine complete view hemispheres (containing 66 spectra each) per sample were acquired. Rotational symmetry must be assumed, since the sun zenith and azimuth angles do not change independently.

Since the target was not only illuminated from one light source (the sun) but also from diffuse sky light, the goniometer did not measure the BRDF, but the so-called hemispherical conical reflectance. A method to determine the BRDF from such a measurement is described in Kriebel (1996). For the comparison with images taken at the same illumination it is not necessary to actually know the BRDF, so this method is not applied. For the clear sky conditions during the Barrax campaign the diffuse illumination is negligible for solar zenith angles of less than 60 degrees and wavelengths above 0.5 µm (Strub, 2000). Therefore the BRDF is reasonably well approximated by the hemispherical conical reflectance.

In order to monitor the atmospheric stability, the atmospheric optical thickness and the amount of water vapour were measured using a Reagan Sun Photometer (Ehsani & Reagan, 1992).

2.1.2 HyMap image spectra

From the total of eight flight lines, only six with clearly different geometries are chosen (c.f., Figure 1). The flight lines are covered at three different times of the day (10, 14 and 17 hrs MET) in a cross-shape pattern with headings of 180 and 270 degrees respectively. The solar position was 'east' at 10 h MET, 'south' at 14 h MET and 'west' at 17 h MET.

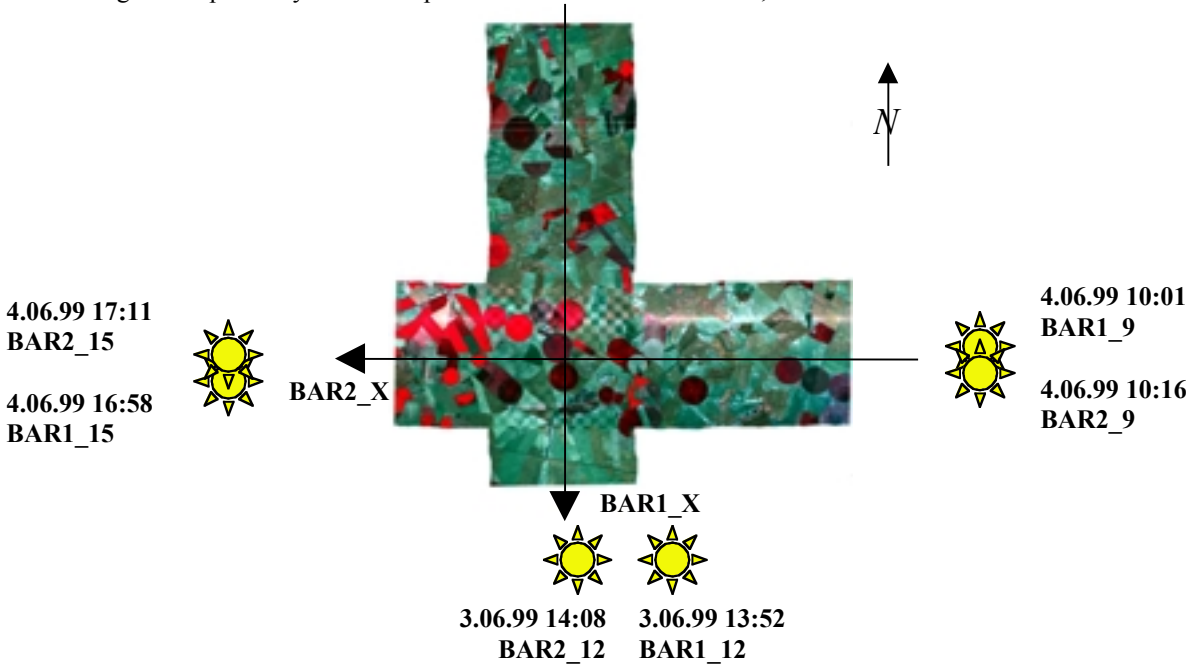

Figure 1. The HyMap flight lines. The sun symbols denote the solar positions for the indicated times and images.

The radiometric calibration of the image data is done by inflight calibration (IFCALI) (Richter, 1996) using the noon image and nadir ground measurements at Barrax. The resulting set of calibration coefficients is used for all scenes.

The image data are atmospherically corrected using the airborne ATCOR4 (Richter, 2000). This compensates the effects of angular dependent path radiance and atmospheric transmittance, as well as the adjacency effect. The algorithm takes into account the different path length of a wide FOV sensor, but uses an isotropic reflectance model.

The scenes are geometrically corrected and geocoded using the PARGE (Schläpfer, 2000).

2.2 Data Analysis

2.2.1 Validation of Reflectance

The most straight forward way of validation is to compare the averaged image spectra at the ground measurement locations to the goniometric spectra from the same view zenith and azimuth angle and the same solar zenith angle.

The image spectra at the ground measurement sites are averaged in a region of interest of about 2.7 degrees, which is the FOV of the ground spectrometer. The view angles are taken from the PARGE output.

The goniometer spectra are resampled to HyMap resolution using the HyMap spectral response functions, and spherically interpolated in three angular dimensions to the viewing geometry of the actual HyMap image pixel viewing geometry.

2.2.2 Validation of Angular Dependence

In order to retrieve soil type specific anisotropy, a spectral classification is performed using SPECL, an add-on-program to ATCOR4. It uses spectral indices and thresholds calculated from the channels corresponding to the TM spectral bands. With this automatic and fast classification algorithm the three goniometer targets can be clearly distinguished. The classification accuracy is tested with a crosscheck of all scenes. Furthermore a SAM classification is performed to check the validity of the spectral classes. The aim is a merely spectral classification not a land use map.

A statistical analysis is performed for each image and each class derived by a separate classification for each image. The lines of constant view zenith angle (the image columns for the N-S flight direction (Bar1_X) and the image lines for the E-W direction (Bar2_X)) are summed up for each class separately, resulting in a mean value and standard deviation for each angle and class.

The statistical mean value contains reflectance variations from the inhomogeneity of the classes as well as view angle effects. The standard deviation reflects the varying pixel frequencies at certain angles as well as inhomogeneity at a constant angle. In order to separate the view angle effects from the variational effects two steps are performed.

First we compare only relative reflectances, i.e. the so-called anisotropy factor (Sandmeier, 1999). The anisotropy factor is defined as the ratio of the directional reflectance to the nadir reflectance. Using the anisotropy factor, the brightness differences between the goniometric samples and the image samples cancel out.

Second, for elimination of brightness variations within the image, an easy-to-invert BRDF model is applied. The fitted curves are then used for comparison. The model used (Ambrals model (Wanner, 1995)) was developed for the 'MODIS BRDF and Albedo Product' (Lucht, 2000b). The usefulness for inversion was demonstrated already by Wanner (1997) and Hu (1997). The Ambrals model is a semiempirical linear kernel based model. Semiempirical means that it is an approximation of a general radiative transfer theory, where the parameters retain some physical meaning, while being linear. Linearity leads to a fast and easy-to-use inversion process (Gauss elimination) with a well developed theory of error estimation (weights of determination) (Lucht, 2000a). A set of angle dependent functions, so-called kernels, is used to model different angular behaviour, while the linear parameters act as weighting of the different effects.

Due to the fast inversion process each spectral band can be inverted independently. However for physical consistency one set of kernels is selected in the end for all channels with individual parameters for each channel. The best subset of kernels (apart from the isotropic kernel usually only one or two) is automatically chosen by comparison of the mean root mean square error of the different fits.

3 RESULTS

3.1 Classification Results for HyMap Data

The classification with SEPCL leads to satisfactory results from the spectral point of view. Speckles within the larger areas are supposed to be a variation in spectral signature caused by areas of sparse vegetation or varying soil moisture and texture. The SAM classification with the same classes gives no significantly different result.

Since the SPECL-algorithm uses not only relative values but also absolute reflectance values, the classification leads to different results for considerably different illumination intensity. This can be seen in the hot spot region of Bar2_12 compared to Bar1_12 where reflectance differs by 50 % (see Figure 2).
Also when comparing Bar1_12 with Bar1_9, the changed sun zenith angle and soil moisture cause some parts of the soil and the dry vegetation to be classified differently (see Figure 3).
But nevertheless, this analysis relies only on homogeneous classes, which can be checked with the standard deviation for each angle and class.

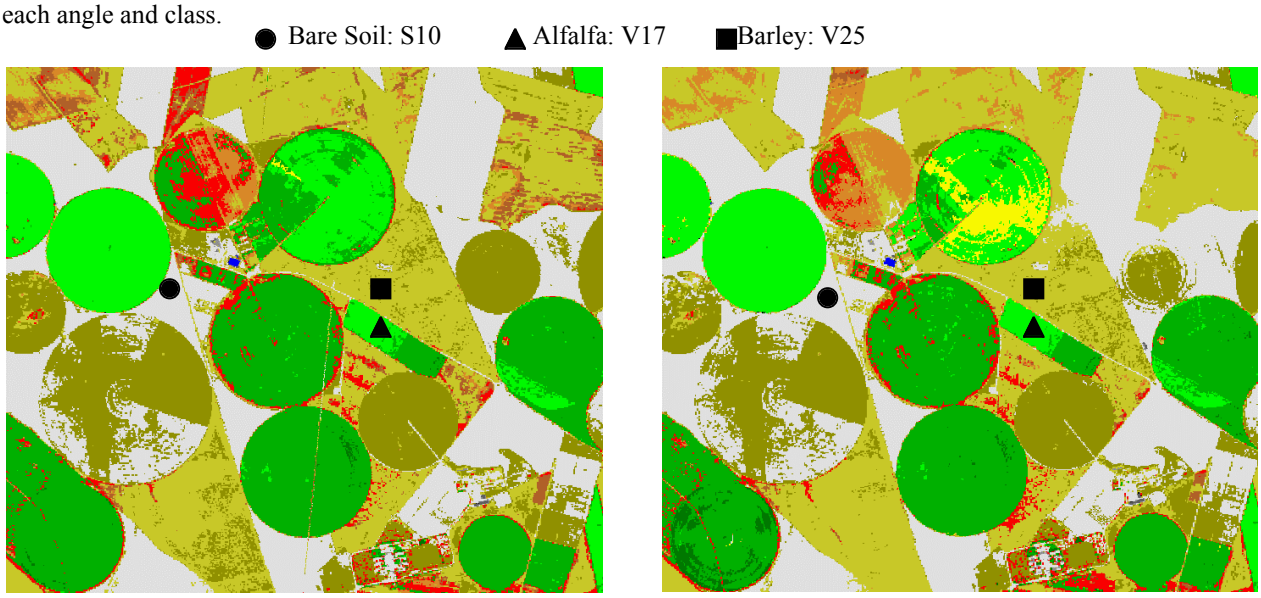

Figure 2. Classification with SPECL at solar zenith angle of 17°.

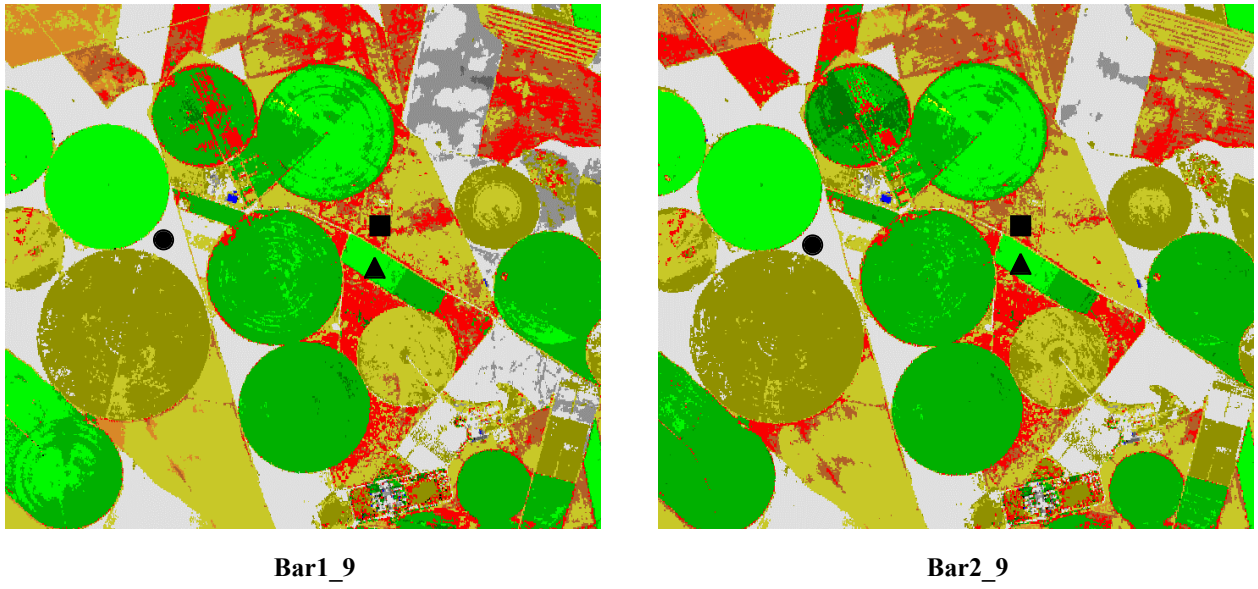

Figure 3. Classification with SPECL at solar zenith angle of 52°.

3.2 Validation of reflectance

The comparison of reflectance values in Figure 4-6 demonstrates the problems of ground measurements (Here only shown for images Bar1_9, Bar1_12 and Bar1_15). While soil spectra are represented well at different angles, alfalfa is systematically misrepresented in the morning and barley is systematically misrepresented at all times of the day. The ground field of view of the ground spectrometer only contained about a dozen ears and their density might not be representative for the whole field.

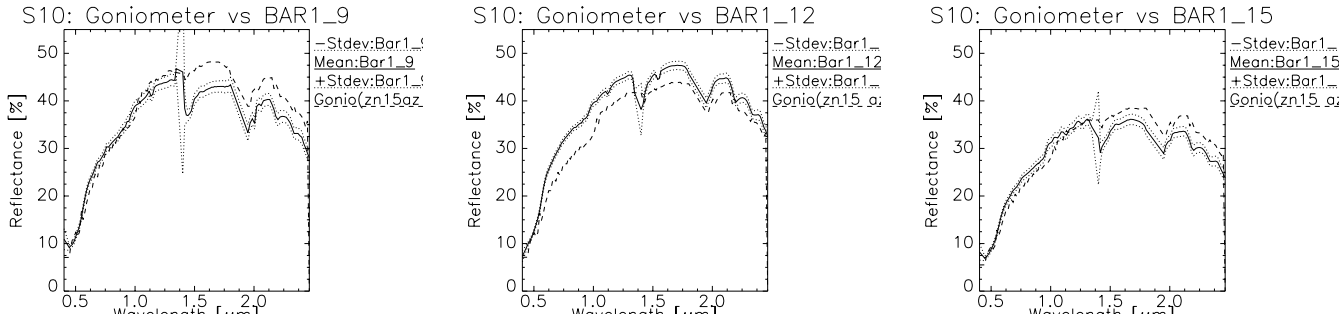

Figure 4. Comparison of S10 image spectra (including standard deviation) with S10 goniometer spectra.

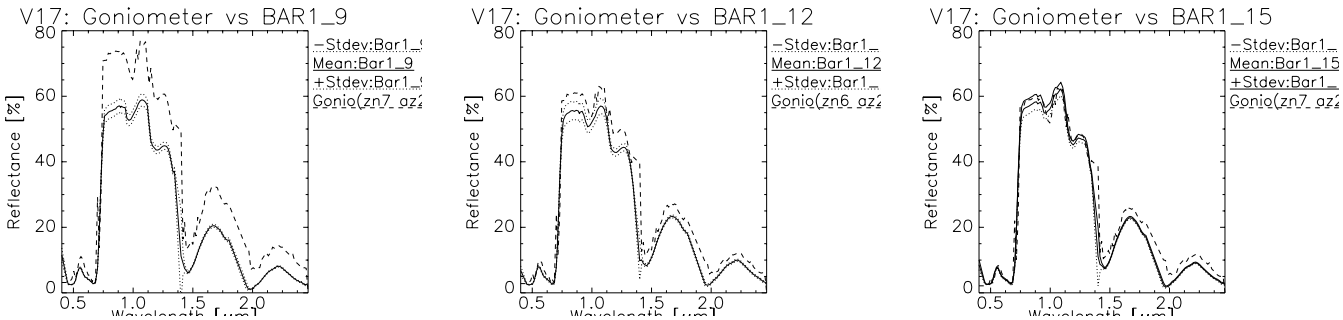

Figure 5. Comparison of V17 image spectra (including standard deviation) with V17 goniometer spectra.

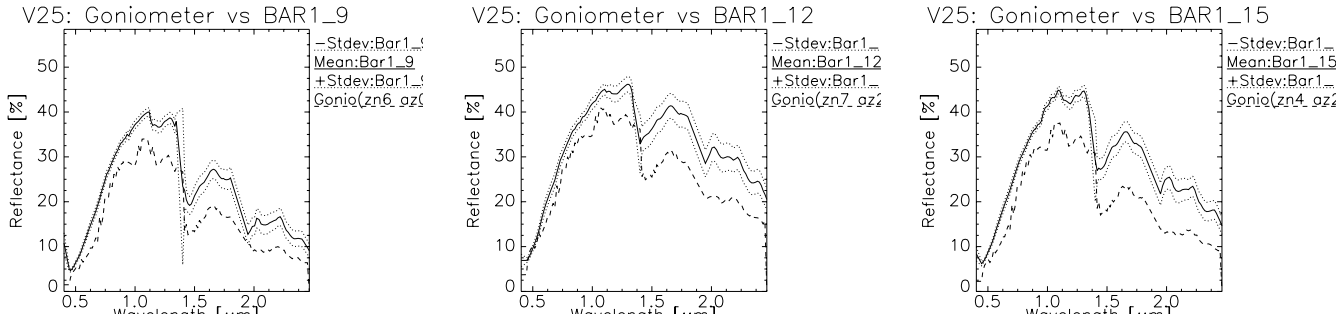

Figure 6. Comparison of V25 image spectra (including standard deviation) with V25 goniometer spectra.

From this comparison it is not possible to decide, whether the disagreement comes from a non-representative sample or a varying angular behaviour.

Furthermore due to restrictions to the fields of the experimental area, the goniometer targets could only be chosen such that they are represented under small view zenith angles in the images (see Table 1). For a complete coverage of the HyMap FOV more targets would have to be measured, which is impractical with the large goniometer. Therefore we present a different approach in the following section.

		S10		V17		V25	
	Solar zenith	View zenith	Relative azimuth	View zenith	Relative azimuth	View zenith	Relative azimuth
Bar1_9	54.1	15.2	180	6.8	16	6.1	15
Bar2_9	51.2	9.1	269	6.1	275	9.1	274
Bar1_12	16.9	15.2	96	6.8	289	6.8	287
Bar2_12	16.8	9.1	175	6.1	181	9.1	187
Bar1_15	40.3	15.5	10	6.8	201	4.3	200
Bar2_15	42.8	6.1	90	6.1	92	9.1	95

Table 1. Illumination and viewing geometry of the goniometer samples.

3.3 Validation of angular dependence

In the following we present a method to compare the goniometric spectra from one target location with the image spectra from the total FOV of the HyMap sensor.

Table 2 shows the standard deviation of the pixels of one class and one view zenith angle averaged over all bands and all view zenith angles. This gives an estimate of the non-angular dependent variability of the classes. The standard deviations within one class are approximately the same for different images (S10: 10%, V17: 17%, V25: 15%). This indicates that the angular dependency has been removed. The standard deviations for the images as a whole are with 39% much larger.

	Bright sand/soil (S10)		Bright vegetation (V17)		Dry vegetation (V25)		Total image	
	# pixel	St. dev.	# pixel	St. dev.	# pixel	St. dev.	# pixel	St. dev.
Bar1_9	66913	11	52264	18	81100	18	436480	42
Bar2_9	78379	12	43908	19	76334	17	436480	42
Bar1_12	96356	10	42142	21	96303	14	436480	36
Bar2_12	106169	8.3	41653	13	107143	12	436480	36
Bar1_15	79256	9.7	56665	14	117557	15	436480	38
Bar2_15	78588	11	44501	15	105771	15	436480	40

Table 2. Number of pixel and mean standard deviation in % of mean reflectance per class.

The BRDF inversion results with the Ambrals model is shown in Table 3 (RLO, etc. denote a specific kernel subtype).

	Bright sand/soil (S10)		Bright vegetation (V17)		Dry vegetation (V25)		Total image	
	Kernel	RMSE	Kernel	RMSE	Kernel	RMSE	Kernel	RMSE
Bar1_9	Li dense RLO	2.1	Li dense RHP	4.2	Li dense RLP	2.8	Ross thick	3.3
Bar2_9	Li dense RLO	2.0	Li dense RLO	2.9	Li dense RLP	2.1	Li transit	2.2
Bar1_12	Li dense RHO	2.2	Ross thick	4	Li dense RLO	1.5	Li transit	3.9
Bar2_12	Li dense RHP	1.2	Li dense RHP	3.3	Li dense RHO	1.5	Li dense RLP	2.6
Bar1_15	Li dense RLO	2.1	Li dense RLP	4.4	Li dense RLP	2.3	Li dense RLP	3.8
Bar2_15	Li dense RLO	1.6	Li dense RLO	2.7	Li dense RLO	2.5	Li transit	2.4

Table 3. Kernel and spectrally averaged inversion RMSEs [%] for the Ambrals model.

The comparison of the angular behaviour of the reflectance for four channels (487nm, 549 nm, 656 nm and 868 nm) is shown in Figures 4-6. The goniometric data are taken with a 15° resolution in view zenith angle. The so-called principal plane measurements (sun, target and observer are in one plane) lack one or two data points due to shadowing of the target by the ground spectrometer.

Taking into account the large standard deviation within each class (cf. table 2) a good agreement between the two angular variations can be found. Only scenes with large sun zenith angles (Bar1_9 and Bar2_15) show larger discrepancies. Those two were taken in the cross-principal plane. Taking only data from this plane, there is not much information content, since the angular dependence is flat for all kernels. Then the Ambrals inversion procedure becomes unstable and produces spurious results.

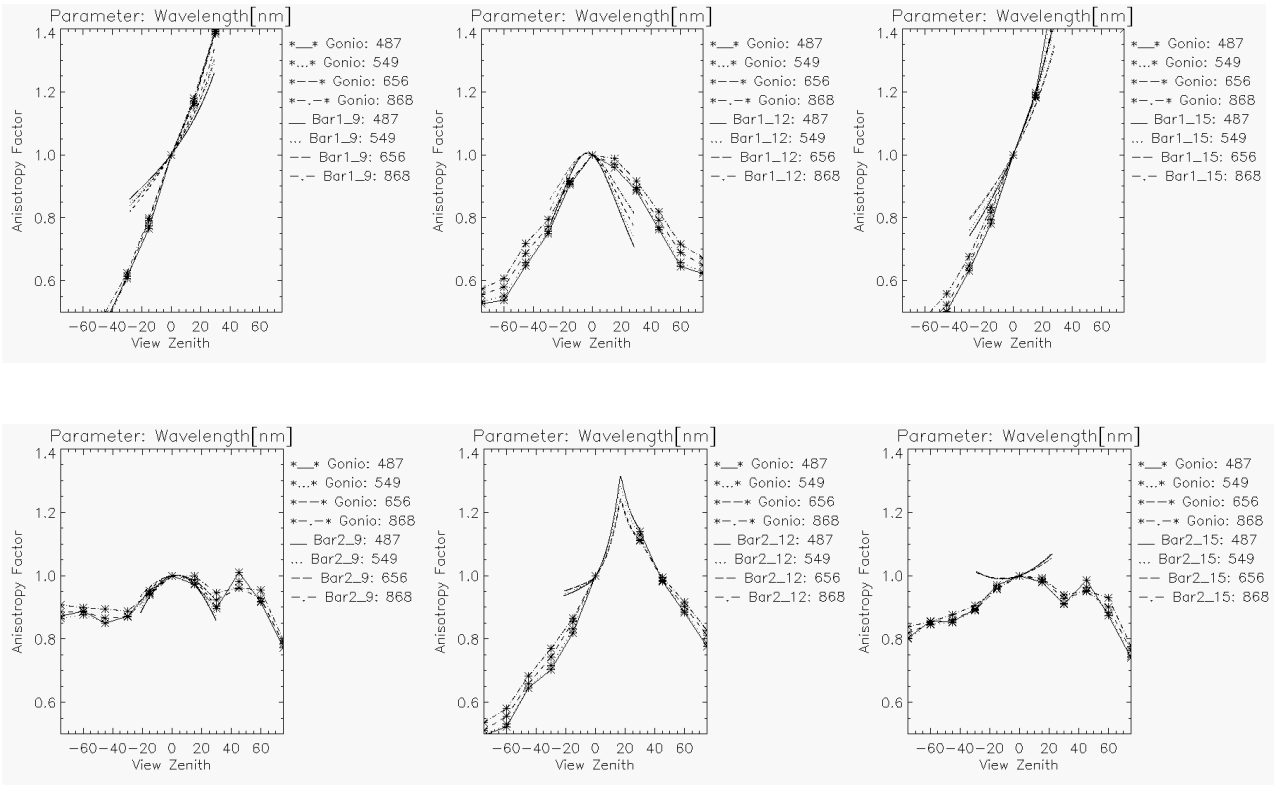

Figure 7. Comparison of anisotropy factors of bright sand/soil with goniometer target S10.

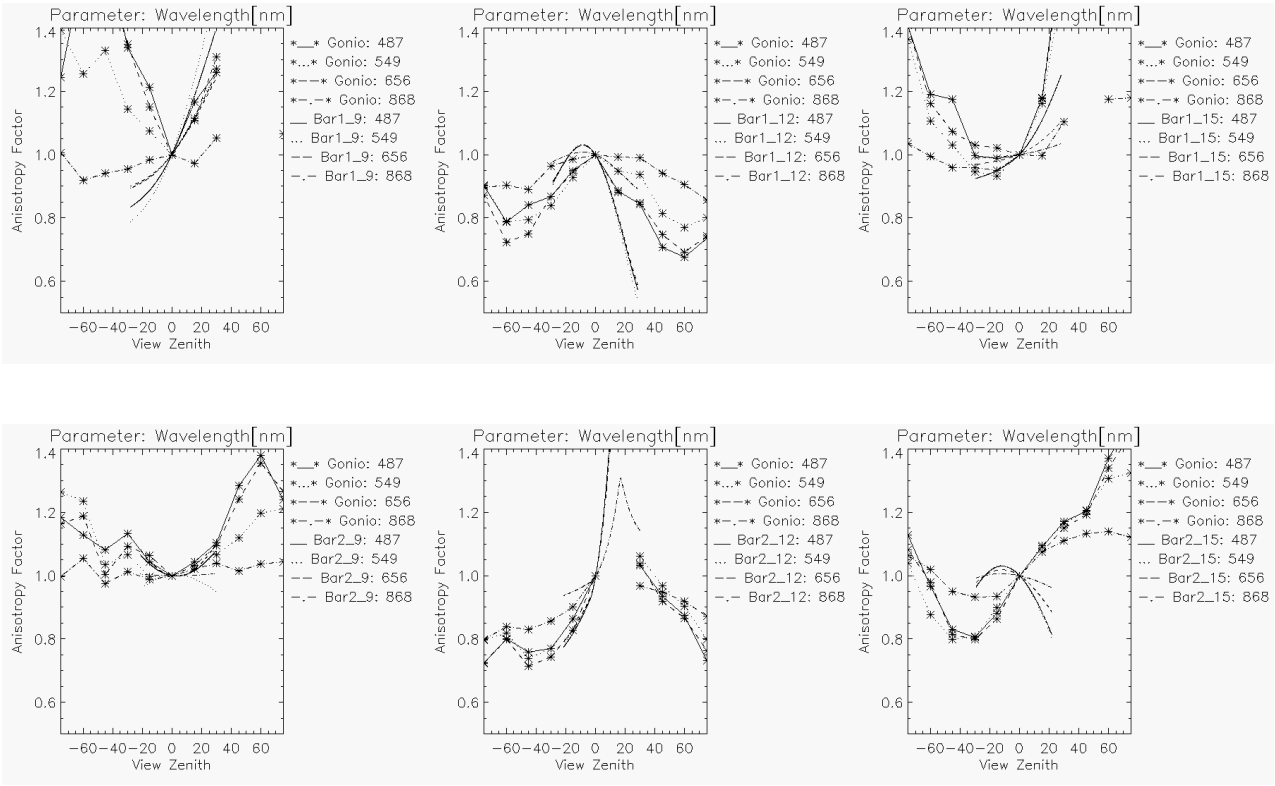

Figure 8. Comparison of anisotropy factors of bright vegetation with goniometer target V17.

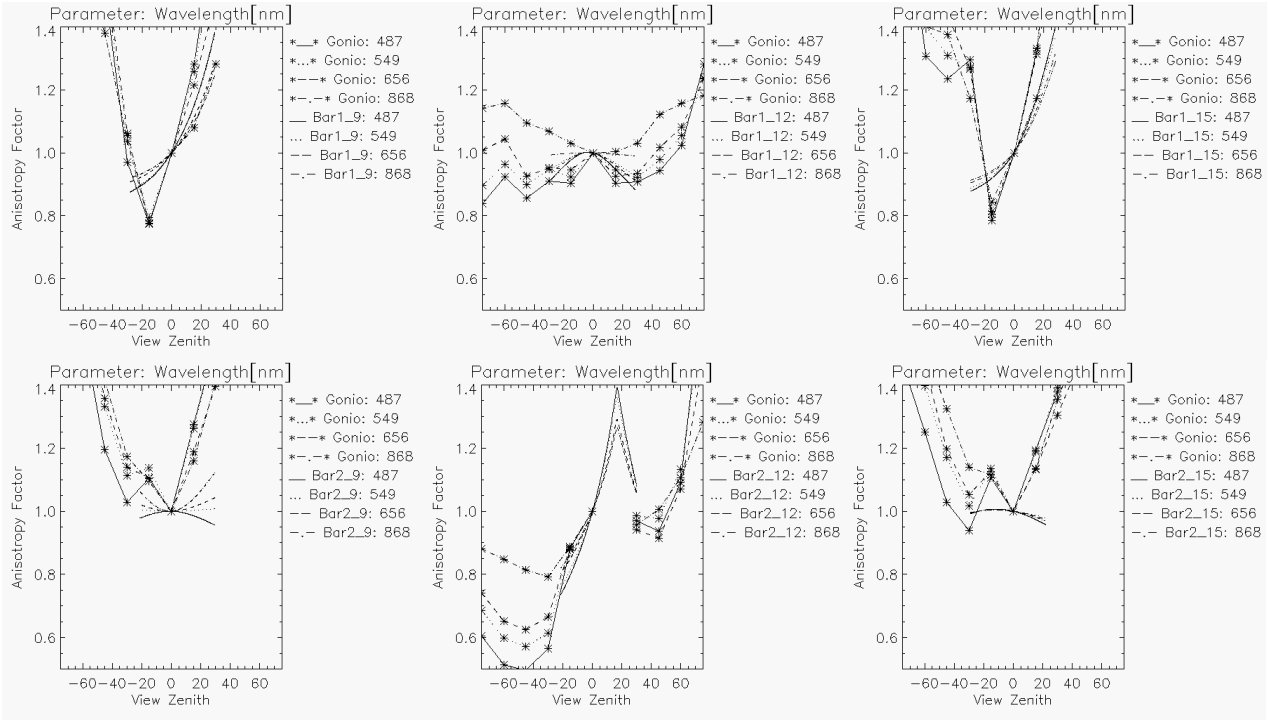

Figure 9. Comparison of anisotropy factors of dry vegetation with goniometer target V25.

4 CONCLUSIONS

In this article we show that the view and illumination angle dependence of spectra within hyperspectral images can be validated with goniometric ground measurements.

A simple ground location to image comparison is not practical, since a large number of ground targets would have to be measured. Therefore a few targets are measured from a large number of view angles covering the whole view hemisphere. This data set was compared to a set of directional spectra derived from statistical averages from hyperspectral images. For each comparison only data from a single image were used.

We can separate the in-scene variation from the angular behavior by dividing up the pixels into spectrally distinct classes and then show that the angular behavior is in good accordance with the ground measurements. This is shown explicitly for three targets: bare soil, green alfalfa and dry barley. The inversion of further classes, obtained from classification, which are not shown here, suggests, that this method is generally applicable. Care must be taken that the number of pixels for a wide range of angles is sufficient. The resulting zenith angle dependence can then be used to correct the images separately for the view angle effect.

So far we have only considered the case of a plane terrain. For uneven terrain a digital elevation model must be used to calculate the sun and view angle relative to the ground normal. This way an even larger angular sampling range can be obtained which helps to find better BRDF inversion coefficients. Unfortunately at the same time it becomes more difficult to find a correct spectral classification.

Although the correction proposed here might not be applicable to all scenes and for all applications, this is a step towards a more accurate quantitative analysis of wide-FOV hyperspectral data and makes it possible to compare data from different times and viewing geometry. This method will reduce flight planning restrictions and make airborne imagery more efficient.

ACKNOWLEDGEMENTS

The authors acknowledge the support and cooperation with the University of Valencia (J. Moreno under ESA contract No. 13390/NL/GD), J.A. Sobrino and coworkers who helped us carrying the goniometer!) and the University of Castilla-LaMancha. The goniometer deployment in Spain was supported by the Univ. of Zurich (RSL). Many thanks to the DLR imaging spectroscopy team (A. Hausold for processing the images, R. Richter for performing the atmospheric

correction and A. Müller/U. Heiden for additional ground measurements). We are very grateful to the MODIS team (esp. W. Lucht) who provided the Ambrals code for BRDF inversion.

REFERENCES

Berger, M., Moreno, J., Müller, A., Schaepman, M., Wursteisen, P., Rast, M. Attema, E., 2000. The Digital Imaging Spectrometer Experiment – DAISEX'99. In Proc. IGARSS 2000, Hawaii, pp. 3039-3041.

Ehsani, A.R., Reagan, J.A., 1992. A Microprocessor Based Auto Sun-Tracking Multi-Channel Solar Radiometer System. In Digest of IGARSS'92, Houston (TX).

ESA, 1999. DAISEX-99 Experimenters Handbook. Draft3, 27 May 1999. ESA Scientific Campaign Unit, ESTEC.

Hu, B., Lucht, W.,Li, X., Strahler, A.H., 1997. Validation of Kernel-Driven Semiempirical Models for the Surface Bidirectional Reflectance Distribution Function of Land Surfaces. Remote Sensing of Environment 62, pp. 201-214.

Kriebel, K.-T., 1996. On the Limited Validity of Reciprocity in Measured BRDFs. Remote Sensing of Environment 58, pp. 52-62.

Lucht, W., Lewis, P., 2000a. Theoretical Noise Sensitivity of BRDF and Albedo Retrieval from the EOS-MODIS and MISR Sensors with Respect to Angular Sampling. International Journal of Remote Sensing 21(1), pp. 81-98.

Lucht, W, Schaaf, C.B., Strahler, A.H., 2000b. An Algorithm for the Retrieval of Albedo from Space Using Semiempirical BRDF Models. IEEE Transactions on Geoscience and Remote Sensing 38(2), pp. 977-998.

Nicodemus, F.E., Richmond, J.C., Hsia, J.J., Ginsberg, I.W., Limperis, T., 1977. Geometrical Considerations and Nomenclature for Reflectance. NBS Monograph 160. U.S. Department of Commerce/National Bureau of Standards.

Richter, R., 1996. Atmospheric Correction of DAIS Hyperspectral Image Data. Computers & Geosciences 22, pp. 785-793.

Richter, R., 2000: A Unified Approach to Parametric Geocoding and Atmospheric/Topographic Correction for Wide FOV Airborne Imagery. Part 2: Atmospheric/Topographic Correction. Proc. 2nd EARSeL Workshop on Imaging Spectroscopy, EARSeL, Enschede.

Sandmeier, S.R., Itten, K.I., 1999. A Field Goniometer System (FIGOS) for Acquisition of Hyperspectral BRDF Data. IEEE Transactions on Geoscience and Remote Sensing 37(2), pp. 978-986.

Schläpfer D., Hausold A., Richter R., 2000. A Unified Approach to Parametric Geocoding and Atmospheric/Topographic Correction for Wide FOV Airborne Imagery. Part 1: Parametric Ortho-Rectification Process. Proc. 2nd EARSeL Workshop on Imaging Spectroscopy, EARSeL, Enschede.

Strub, G., Beisl, U., Schaepman, M., Schläpfer, D., Dickerhof, C., Itten, K., 2000. Evaluation of Diurnal Hyperspectral BRF Data Acquired with the RSL Field Goniometer During the DAISEX '99 Campaign. Proc. 2nd EARSeL Workshop on Imaging Spectroscopy, EARSeL, Enschede.

Wanner, W., Li, X., Strahler, A.H., 1995. On the Derivation of Kernels for Kernel-driven Models of Bidirectional Reflectance. Journal of Geophysical Research 100(D10), pp. 21077-21089.

Wanner, W., Strahler, A.H., Hu, B., Lewis, P., Muller, J.-P., Li, X., Barker Schaaf, C.L., Barnsley, M.J., 1997. Global Retrieval of Bidirectional Reflectance and Albedo over Land from EOS MODIS and MISR Data: Theory and algorithm. Journal of Geophysical Research 102(D14), pp. 17143-17161.